U-13C-glucose incorporation into source leaves of Brassica napus highlights light-dependent regulations of metabolic fluxes within central carbon metabolism

Younès Dellero, Solenne Berardocco, Alain Bouchereau

Article

U-^{13}C-glucose incorporation into source leaves of *Brassica napus* highlights light-dependent regulations of metabolic fluxes within central carbon metabolism

Younès Dellero [1 *], Solenne Berardocco [2] and Alain Bouchereau [2]

[1]INRAE, Université Rennes, Institut Agro, IGEPP-UMR1349, P2M2-MetaboHUB, Le Rheu, 35653, France

[2]Université Rennes, INRAE, Institut Agro, IGEPP-UMR1349, P2M2-MetaboHUB, Le Rheu, 35653, France

[*]Corresponding author: younes.dellero@inrae.fr

Abstract: Plant central carbon metabolism comprises several important metabolic pathways acting together to support plant growth and yield establishment. Despite the emergence of ^{13}C-based dynamic approaches, the regulation of metabolic fluxes between light and dark conditions has not yet received sufficient attention for agronomically relevant plants. Here, we investigated the impact of light/dark conditions on carbon allocation processes within central carbon metabolism of *Brassica napus* after U-^{13}C-glucose incorporation into leaf discs. Leaf gas-exchanges and metabolite contents were weakly impacted by the leaf disc method and the incorporation of glucose. ^{13}C-analysis by GC-MS showed that U-^{13}C-glucose was converted to fructose for *de novo* biosynthesis of sucrose at similar rates in both light and dark conditions. However, light conditions led to a reduced commitment of glycolytic carbons towards respiratory substrates (pyruvate, alanine, malate) and TCA cycle intermediates compared to dark conditions. Analysis of ^{13}C-enrichment at the isotopologue level and metabolic pathway isotopic tracing reconstructions identified the contribution of multiple pathways to serine biosynthesis in light and dark conditions. However, the direct contribution of the glucose-6-phosphate shunt to serine biosynthesis was not observed. Our results also provided isotopic evidences for an active metabolic connection between the TCA cycle, glycolysis and photorespiration in light conditions through a rapid reallocation of TCA cycle decarboxylations back to the TCA cycle through photorespiration and glycolysis. Altogether, these results suggest the active coordination of core metabolic pathways across multiple compartments to reorganize C-flux modes.

Keywords: *Isotope, tricarboxylic acid cycle, glycolysis, serine, carbon isotopologue distribution, light, dark, Brassica napus*

Abbreviations: GC-MS, Gas Chromatography Mass Spectrometry; CID, Carbon Isotopologue Distribution; TCA, Tricarboxylic acid; PEPC, Phosphoenolpyruvate carboxylase; PDH, Pyruvate dehydrogenase.

1. Introduction

Central carbon metabolism comprises several essential metabolic pathways to sustain plant growth and development, such as the Calvin-Benson-Bassham cycle, the pentose phosphate pathway, photorespiration, sucrose and starch metabolisms, glycolysis, the tricarboxylic acid (TCA) cycle and lipid metabolism [1]. These pathways are coordinated together along with nutrient acquisition to fuel primary metabolism for biomass production, reproduction and acclimation to environmental cues [2-5]. However, climate change negatively impacts physiological processes and their associated metabolic pathways, hence reducing the yield potential of future crop productions [6]. While the engineering of plant central carbon metabolism has been successfully deployed in recent years [5, 7-9], important regulatory hubs and key metabolic steps remain unidentified [10, 11]. Indeed, regulation of plant primary metabolism at the transcriptomic and proteomic levels is not often correlated with intuitive variations of metabolite pools and their associated metabolic fluxes [12-14]. Over the last years, dynamic studies of plant central carbon metabolism through the tracing of radioactive and stable carbon isotopes (^{14}C and ^{13}C, respectively) have largely contributed to a better understanding of regulating processes in different environmental conditions and in different organs [15-25].

Plant ^{13}C-labelling strategies are based on either a global approach using $^{13}CO_2$ or targeted approaches using ^{13}C-labelled metabolic substrates [26]. Overall, $^{13}CO_2$-based metabolic flux analyses have successfully described allocation patterns of newly assimilated carbon in the light to the Calvin cycle, sugar and starch biosynthesis, glycolysis, the TCA cycle and nitrogen assimilation [4, 16, 18, 23, 27, 28]. However, this approach cannot be used to explore central carbon metabolism in non-phototrophic tissues or in non-photosynthetic conditions [26]. Targeted approaches combining different ^{13}C-labelled metabolic substrates with Arabidopsis mutants provided important new insights into plant metabolism in the light [29]. Such studies led to discoveries including: i) The occurrence of three pyruvate-supplying pathways for respiration, ii) the central role of malate-citrate exchanges for the TCA cycle, and iii) the involvement of specific thioredoxins in regulating carbon flow through the TCA cycle [30-34]. The inhibition of TCA cycle activity in the light also relied on the restriction of carbon flux towards glycolysis and the inhibition of TCA cycle dehydrogenases by photorespiratory-produced metabolites in mitochondria [2, 3, 16]. Notably, the restrictive role of glycolysis was supported by: i) The inhibition of pyruvate dehydrogenase (PDH) activity in the light [35], ii) a higher inhibition of PDH and TCA cycle decarboxylations the light when using ^{13}C-glucose compared to ^{13}C-pyruvate [36]. However, a recent ^{13}C-labelling study in Arabidopsis questioned the importance of PDH in restricting glycolytic carbon flux towards the TCA cycle in the light. Indeed, no differences of ^{13}C-redistribution in TCA cycle intermediates were observed between a *pdk* mutant (PDH activated) and control plants after incorporation of either U-^{13}C-glucose or U-^{13}C-pyruvate under light conditions [37]. To date, targeted approaches in both light and dark conditions have been essentially deployed in guard cells [17, 38-40] rather than in whole leaf tissues [41, 42]. Thus, the regulation of TCA cycle activity by glycolytic carbon flux remained to be investigated in leaf tissues.

Winter oilseed rape (*Brassica napus*) is a major oleaginous crop, important for human and animal nutrition and biofuel production (seed oil and cake) [43, 44]. However, its crop cycle requires an important amount of mineral nitrogen to achieve maximal seed yield compared to other oleaginous crops [45, 46]. Indeed, *B. napus* has a high nitrogen utilization efficiency but a low nitrogen remobilization efficiency [47, 48]. Since TCA cycle activity partially supports nitrogen assimilation in the light, the regulation of central carbon metabolism in *B. napus* leaves could substantially differ compared to other crops. Furthermore, *B. napus* can face different environmental stress combinations throughout its crop cycle, including intermittent shade, which will decrease nitrogen assimilation, sugar transport and ultimately seed yield [49]. Therefore, the identification of carbon allocation processes within central carbon metabolism of *B. napus* leaves under light and dark conditions is an important prerequisite for studying the metabolic adaptation of *B. napus* to intermittent shade. To date, few works have investigated central carbon metabolism of *B. napus* in light and dark conditions. It has been proposed that the TCA cycle was fed essentially by stored citrate in the light [27]. However, this conclusion also questioned the occurrence of metabolic connections between chloroplasts and mitochondria in the light and the inhibition of TCA cycle activity by a reduced glycolytic flux in *B. napus* leaves. Recently, incorporation of U-^{13}C-pyruvate into *B. napus* leaf discs under both light and dark conditions raised some doubts concerning the possible contribution of a stored citrate pool to mitochondrial TCA cycle functioning [42]. In addition, it was proposed that TCA cycle decarboxylations could be reassimilated by Rubisco and reallocated to photorespiratory intermediates, thereby reinforcing metabolic connections between cell organelles in the light. However, some interactions may have been missed by our experimental setup. The use of pyruvate necessarily restricted the entry of chloroplastic 3-phosphoglycerate into mitochondrial pyruvate. Leaf discs floating on a liquid could also be prone to severe photorespiratory conditions, leading to the description of non-physiological metabolic interactions. Finally, the glycolytic regulation of TCA cycle activity was not observed, *i.e.* there were no differences of ^{13}C-enrichments in TCA cycle intermediates between light and dark conditions.

The objectives of this study were: (1) To validate the physiological relevance of *B. napus* leaf discs for studying central carbon metabolism under light and dark conditions, (2) to evaluate the contribution of glycolysis to TCA cycle activity in light and dark conditions, (3) to identify metabolic interactions between different pathways of central carbon metabolism under light and dark conditions. For this purpose, we incorporated U-^{13}C-glucose into *B. napus* leaf discs for up to 6 h in either light or dark conditions and performed gas-exchange measurements. Then, the relative levels of central metabolites (sugars, organic and amino acids) were measured and their ^{13}C-enrichments determined by gas-chromatography mass spectrometry (GC-MS). Isotopic analysis identified important differences in carbon allocation processes in *B. napus* leaves in response to light availability.

2. Methods

2.1 Plant growth and chlorophyll estimations

Brassica napus genotype Aviso was grown for two months at a photosynthetic photon flux density of 100-150 µmol photons.m^{-2}.s^{-1} in conditions described previously [13]. All experiments were performed on the mature leaf L9 (source status) of plants grown for up to 60 days after sowing. At this stage (BBCH-19), the two first leaves (L1 and L2) had already fallen. The stage of the leaf was also confirmed by measuring the chlorophyll index in SPAD units (mean of 36.6 ± 0.98). Plants received 4 h of light prior starting experiments.

2.2 Gas-exchange measurements

Net CO_2 assimilation and dark respiration were measured on either a leaf attached to the plant or leaf discs. Gas-exchange measurements were performed with a portable photosynthesis system (LI 6800-F, LiCOR, Lincoln, Nebraska, USA). Standard measuring conditions were: 120 µmol photons.m^{-2}.s^{-1} of light intensity, a leaf temperature of 25-26°C, 65-80% relative humidity (leaf VPD ranging from 0.8 to 1.2), 430 µL CO_2.L^{-1} and 0.21 L O_2.L^{-1}. Steady-state parameters were measured after 30-45 min of light (net CO_2 assimilation) followed by 20-30 min of dark (dark respiration). Measurements on attached leaves were performed with a 6800-01A chamber (LiCOR) comprising a light source. After measurements, 20-30 leaf discs (0.8 cm^2) were taken from the attached leaf and incubated for 5 min in a petri dish containing 30 mL of 10 mM MES-KOH (pH 6.5). Then the petri dish was placed into a custom chamber connected to the LI 6800-F using the 6800-19 Custom Chamber Adapter (LiCOR; **Figure S1**). The custom chamber had a volume of 1-1.4 dm^3, contained 4 small fans that allowed a 95% air renewal in approximately 2 min. The custom chamber was placed under a light source (120 µmol photons.m^{-2}.s^{-1}) and on a magnetic stirrer to allow a moderate orbital shaking of leaf discs. For other experiments, leaf discs were incubated in the same conditions described for U-^{13}C-glucose incorporations (section 2.3). Gas-exchange measurements were performed before the incubation (T0) and after either 6 h of light (CO_2 assimilation) or 6h of dark (dark respiration). Steady-state parameters were measured after 15-30 min of adaptation to the custom chamber.

2.3 U-^{13}C-D-glucose incorporations

For each labelling kinetic, 66 leaf discs of 0.8 cm^2 were taken and incubated in a 10 mM MES-KOH (pH 6.5) buffer for 15 min to avoid leaf dehydration. Labelling was initiated by incubating leaf discs with the same buffer containing 10 mM $^{13}C_6$-D-glucose (^{13}C isotopic purity of 99%, Cambridge Isotope Laboratories (Eurisotop, France)). Each time point (0.5, 1, 2, 4, 6 h) corresponded to the incubation of 6 leaf discs in a well (of a 6-well microplate) containing 4 mL/well of ^{13}C-labelled buffer. For timepoint 0, leaf discs were directly harvested in liquid nitrogen prior to the incubation procedure. All incubations were performed at 20 °C with 70 rpm orbital shaking under either a continuous light of 120 µmol photons.m^{-2}.s^{-1} or under dark conditions using multiple opaque plastic bags, similar to a previous experimental set-up used for dark-induced senescence [14]. Sampling was done by freezing leaf discs in liquid nitrogen after a rinsing step (3 times 10 s in a neutral buffer (10 mM MES-KOH (pH 6.5)).

2.4 Measurements of Carbon Isotopologue Distribution (CID) and metabolite contents by GC-MS

Polar metabolites were extracted in a mixture of methanol/chloroform/water containing 200 µM adonitol (internal standard) as described in [13]. Sample derivatization, metabolite identification/analysis by GC-MS and carbon isotopologue distribution (CID) analysis have been described in detail elsewhere [42]. Briefly, metabolites were derivatized with methoxyamine (MEOX) and N-methyl-N-(trimethylsilyl)-trifluoroacetamide (MSTFA), producing MEOX-TMS and TMS derivatives. Then derivatized metabolites were separated on a GC-MS device (TG-5MS column), followed by ionization by electronic impact (70 eV) and mass spectra analysis. Samples were analysed in three runs, each containing additional controls such as alkane mixtures (C7 to C40) for retention time recalibration and mixtures of derivatized authentic standards for metabolite identification according to retention time index and mass spectra (**Table S1**). The second eluted peak (corresponding to isomer 2) was used for both Glucose_MEOX5TMS and Fructose_MEOX5TMS given that plant extracts lacked the isomer 1 for Glucose_MEOX5TMS in our experiments. Integration of CID for organic and amino acids was performed for specific TMS-derivatives, which produced mass fragments previously validated for their accuracy in ^{13}C-labelling measurements [42]. For glucose, fructose and sucrose, mass fragments harbouring carbon skeletons identified in previous studies were used: m/z 160 (C1-C2) and 319 (C3-C6) for Glucose_MEOX5TMS, m/z 364 (C1-C4) and 307 (C4-C6) for Fructose_MEOX5TMS and m/z 361 (60% C1-C6 and 40 % C7-C12), 437 (C8C12 only) and 451 (C7C12) for sucrose_8TMS [50-53]. The relative contribution of fructosyl and glucosyl moieties of Sucrose_8TMS to the m/z 361, 437 and 451 was measured using sucrose-D(fructose-$^{13}C_6$) and sucrose-D(glucose-$^{13}C_6$) (^{13}C isotopic purity of 98%, Cambridge Isotope Laboratories (Eurisotop, France)) injected at 300 µM on our GC-MS set-up (**Figure S2**). The isotopic pollution previously observed for Glucose_MEOX5TMS_C1C2 [34] was checked by examining glucose, 1,2-$^{13}C_2$-glucose and U-^{13}C-glucose (^{13}C isotopic purity of 98%, Cambridge Isotope Laboratories (Eurisotop, France)) on our GC-MS (**Figure S3**). The isotopic pollution was corrected using the known isotopic distribution for the Glucose_MEOX5TMS_C3C6 fragment, but the mathematical framework proposed in a previous work [34] was modified. Our corrective step was performed on raw areas and by considering the isotopic pollution generated by the natural isotopic abundance of each fragment used (see **Figure S4**). Raw areas of CID were corrected for the contribution of naturally occurring isotopes and normalized to the ^{13}C abundance of the tracer with a specific GC-MS dedicated methodology [54, 55]. An **example file** for GC-MS outputs is given in **supplemental files** to help the reader to reproduce the method on their own instrument. In this file, the fragment names already contain information about the metabolite targeted, its derivatives, the isotopic cluster associated and the m/z used. Fractional CIDs and mean ^{13}C enrichments were directly obtained from IsoCor outputs (isotopologue_fraction and mean_enrichment) (see dataset in **Table S2**). For metabolite content measurements, corrected areas of isotopologues were summed for each isotopic cluster of each fragment. The summed areas were normalized to the area of the internal standard (adonitol) and to the sample dry weight, giving relative unit values (relative amount per gDW). Finally,

metabolite contents were normalized to the experimental time 0 (mean value set to 1) and expressed as Log2 fold-changes.

2.5 Data management, visualization and statistical analysis

Raw data were retreated and visualized using custom R scripts based on the packages tidyr, dplyr, ggplot2 [56-58]. All values are expressed as the mean ± standard deviation (SD) from 4 biological replicates (^{13}C-kinetics) or 4-6 biological replicates (gas exchange measurements). For leaf gas exchange measurements, comparison of two groups of means was achieved with a student test (p-value < 0.05, equal variances, bilateral assumptions) while comparison of multiple groups of means was achieved with a one-way ANOVA (p-value < 0.05). For relative metabolite levels and mean ^{13}C enrichments, statistical analysis of the two factors and their interactions were evaluated with a two-way ANOVA test (p-value < 0.05). Post-hoc tests were focused on a single effect and either i) a student test (p-value < 0.05, equal variances, bilateral assumptions) was used to compare light and dark conditions at each time point, or ii) a post-hoc Tukey HSD test (p-value < 0.05) was used to identify isotopologue groups that were significantly different at each time point. All statistical tests were carried out using the built-in functions (package "Stats") of Rstudio *v2022.07.2 build 576* [59].

3. Results

3.1. Incorporation of U-^{13}C-glucose into *B. napus* leaf discs introduced minor variations of net CO_2 assimilation and metabolite contents but not dark respiration

A comparison of gas-exchange measurements of attached leaves and leaf discs performed at the same light intensity showed minor differences. Net CO_2 assimilation was significantly reduced by up to 18% in leaf discs compared to attached leaves (4.6 versus 5.6 µmol $CO_2.m^{-2}.s^{-1}$) however dark respiration was not significantly changed (**Figure 1A**). The 6 h kinetic time course and the incubation with glucose did not introduce any additional variations of these parameters (**Figure 1B**). Following U-^{13}C-glucose incorporations, the levels of glucose and fructose were not significantly modified in both light and dark conditions (metabolic pseudo steady-state), perhaps reflecting the presence of large pre-existing pools (**Figure 1C**). Therefore, glucose levels remained at physiological concentrations in leaf discs throughout the kinetic experiment. Besides this, the levels of sucrose, alpha-alanine and aspartate decreased slightly but significantly during the 6 h period while the level of succinate increased significantly. Serine and malate levels were significantly altered during the time course of the kinetic experiment but this essentially depended on the light/dark condition (significant interaction *CxT*). Some minor but significant differences were observed between light and dark conditions for succinate, aspartate and serine, as previously described in other experiments with *B. napus* leaf discs [42]. It should be noted that some important metabolic markers of stress response were not observed: i) An accumulation of alpha-alanine (hypoxia stress) [60], ii) an accumulation of glycine (highly photorespiratory conditions) [61-63]. Overall, U-^{13}C-glucose incorporations into *B. napus* leaf discs only weakly impacted the activity of core leaf metabolic pathways (photosynthesis, photorespiration and respiration). Therefore, the experimental setup was used to study the impact of light availability on *B. napus* central carbon metabolism.

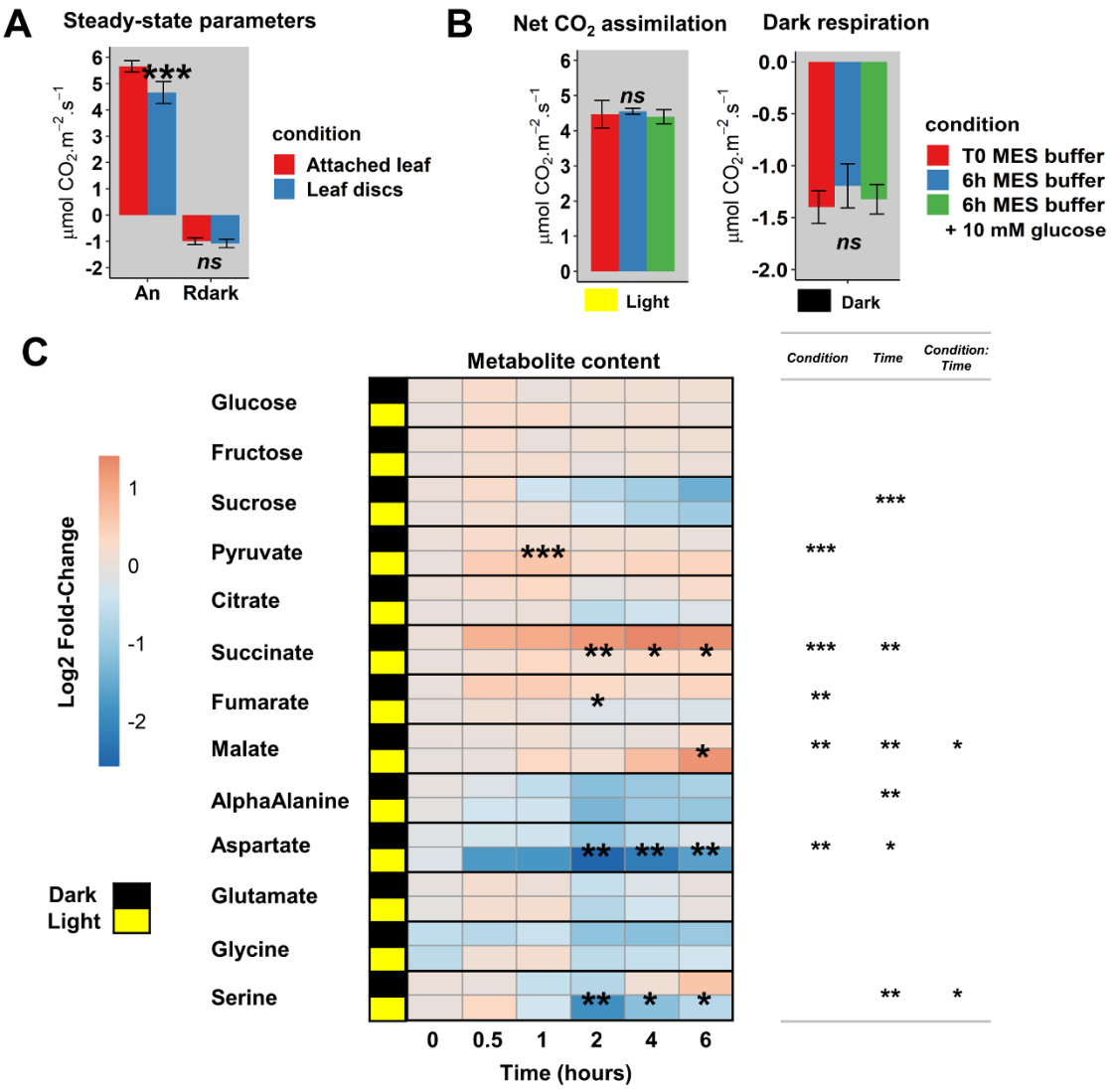

Figure 1. Gas-exchange measurements and metabolite contents of *B. napus* leaf discs fed with 10 mM U-^{13}C-glucose for up to 6 h under light and dark conditions. (**A**) Comparison of net CO_2 assimilation (An) and dark respiration (Rdark) for attached leaves and leaf discs, (**B**) Net CO_2 assimilation (An) and dark respiration (Rdark) of leaf discs before and after 6 h of glucose incorporation, (**C**) Heatmap representation of relative metabolite levels during the time course of U-^{13}C-glucose incorporation. Metabolite contents were normalized to the internal standard adonitol and sample dry weights and expressed as log2 fold-changes with respect to time 0 of the experiment (coloured boxes represent the mean values (n=4). Values for gas-exchange measurements represent the mean ± SD (n=4-6). Statistical differences for gas-exchange measurements were assessed with a Student's t-test (***, p-value<0.001) for (A) and a one-way ANOVA (p-value<0.05, ns: not significant) for (B). For relative metabolite levels, the effect of the two factors ("condition" (*C*) and "time" (*T*)) and their interactions (*CxT*) was assessed with a two-way ANOVA (ns: not significant; *, p-value<0.05; **, p-value<0.01; ***, p-value<0.001). When *C* and/or *CxT* effects were significant, statistical differences between light and dark conditions were assessed at each time point with a Student's t-test, denoted with black stars (*, p-value<0.05; **, p-value<0.01; ***, p-value<0.001). Relative metabolite levels are given in **Figure S5**.

3.2. Redistribution of U-^{13}C-glucose within TCA cycle intermediates identified glycolysis as a major contributor to light-dependent inhibition of TCA cycle activity

To investigate carbon allocation processes between glycolysis, the TCA cycle and photorespiration, ^{13}C-enrichment in some sugars, organic and amino acids was analysed by GC-MS for each time point during U-^{13}C-glucose incorporation. Overall, mean ^{13}C enrichment was increased during the kinetic time course for most of the metabolites detected ("T" effect at p-value<0.001) (**Figure 2**). For Glucose_MEOX5TMS, the mean ^{13}C-enrichement increased rapidly for fragments C1C2 and C3C6 until 30 min and then reached an isotopic pseudo steady-state (**Figure 2A**). Given the metabolic pseudo steady-state observed for glucose (**Figure 1C**), U-^{13}C-glucose uptake by leaf discs was relatively similar between light and dark conditions. Conversely, mean ^{13}C-enrichment in fructose and sucrose fragments showed a progressive and significant increase over time for both conditions. Only fructose showed a significantly higher enrichment in light conditions after 4 h and 6 h compared to dark conditions. Interestingly, mean ^{13}C-enrichment in glycolysis and TCA cycle organic acids (pyruvate, citrate, succinate, malate) was significantly higher in dark conditions compared to light conditions (**Figure 2B**). A number of differences were observed from 2 h that became more important up to 6 h. There were no statistically significant differences for fumarate, perhaps due to its weak detection accuracy as previously observed in *B. napus* leaves [42]. Mean ^{13}C-enrichment in some TCA cycle-derived amino acids (alpha-alanine, glutamate and aspartate) followed the same trend observed for organic acids. However, significant differences were already seen after only 1 h (**Figure 2C**). Mean ^{13}C-enrichment in photorespiratory intermediates (glycine and serine) increased in light conditions, thereby reflecting the previously reported reassimilation of PDH and TCA cycle decarboxylations [42]. In dark conditions, mean ^{13}C-enrichment in serine also increased while the mean ^{13}C-enrichment in Glycine_3TMS_C2 was significantly lower after 6 h compared to light conditions. Thus, the commitment of U-^{13}C-glucose to serine biosynthesis in the dark was probably independent of glycine. To summarize, light conditions drastically reduced the reallocation of glycolytic carbons towards respiratory substrates (pyruvate, alanine, malate) and TCA cycle intermediates compared to dark conditions. Since U-^{13}C-glucose uptake was similar between light and dark conditions, the regulation of glycolysis by light availability largely contributed to the inhibition of the TCA cycle in the light. Conversely, redistribution of ^{13}C towards serine biosynthesis was similar in light and dark conditions but appeared to involve different pathways due to the absence of photorespiration in the dark. To evaluate the contribution of metabolic pathways to the mean ^{13}C-enrichment measured, we analysed the carbon isotopologue distribution (CID) of each fragment.

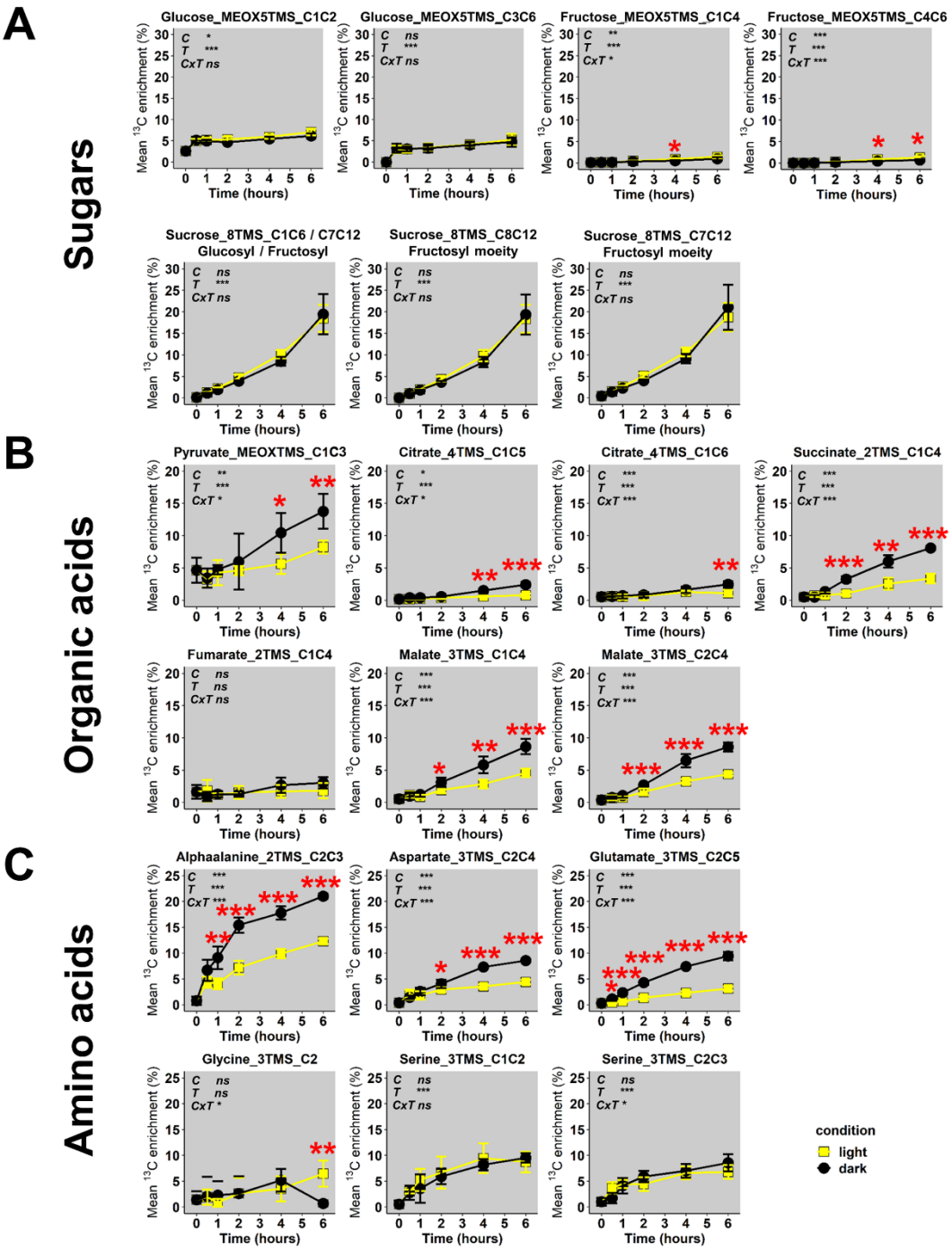

Figure 2. Mean ^{13}C enrichment in sugars, organic and amino acids of *B. napus* leaf discs fed with 10 mM U-^{13}C-glucose for up to 6 h under light and dark conditions. Mean ^{13}C enrichment for **(A)** sugars, **(B)** organic acids and **(C)** amino acids. Values represent the mean ± SD (n=4). The effect of the two factors ("condition" (*C*) and "time" (*T*)) and their interactions (*CxT*) was assessed with a two-way ANOVA (ns: not significant; *, p-value<0.05; **, p-value<0.01; ***, p-value<0.001). When *C* and/or *CxT* effects were significant, statistical differences between light and dark conditions were assessed at each timepoint with a Student's t-test, denoted with red stars (*, p-value<0.05; **, p-value<0.01; ***, p-value<0.001). The complete dataset in available in **Table S2**.

3.3. Contribution of both $^{13}C_6$-glucose and $^{13}C_6$-fructose to sucrose biosynthesis

Analysis of CID in Glucose_MEOX5TMS identified an analytical bias for the M1 isotopologue of the C1-C2 fragment, leading to a constant abundance of 5% starting from the time point 0. Nevertheless, there were some important increases of fully labelled Glucose_MEOX5TMS fragments (M2 isotopologue of C1C2 and M4 isotopologue of C3C6) during the kinetic analysis in both light and dark conditions (**Figure 3A**). Thus, there was no significant rearrangement of label in glucose during the experiment. Fully labelled fragments of Fructose_MEOX5TMS were also dominantly increased during the kinetic time course in both conditions (M4 isotopologue for C1C4 and M3 isotopologue for C4C6). Regarding the biosynthesis of sucrose (glucose + fructose), we also observed dominant increases for fully labelled fragments of Sucrose_8TMS: M6 isotopologue of C7C12 fructosyl, M5 isotopologue of C8C12 fructosyl and M6 isotopologue of C1C6glucosyl/C7C12fructosyl (**Figure 3B**). There was a 60/40 ratio for the contribution of glucosyl/fructosyl moieties in Sucrose_8TMS_ C1C6glucosyl/C7C12fructosyl (**Figure S2**). Thus, the maintenance of similar abundances for the M6 isotopologue of C7C12 fructosyl and C1C6glucosyl/C7-C12 fructosyl fragments clearly confirmed that both $^{13}C_6$-glucose and $^{13}C_6$-fructose were used for sucrose biosynthesis (**Figure 3C**). Mean ^{13}C enrichment of sucrose was much higher compared to glucose and fructose (20% versus 1-4% at 6 h) probably due to the presence of inactive non-labelled pools of glucose and fructose.

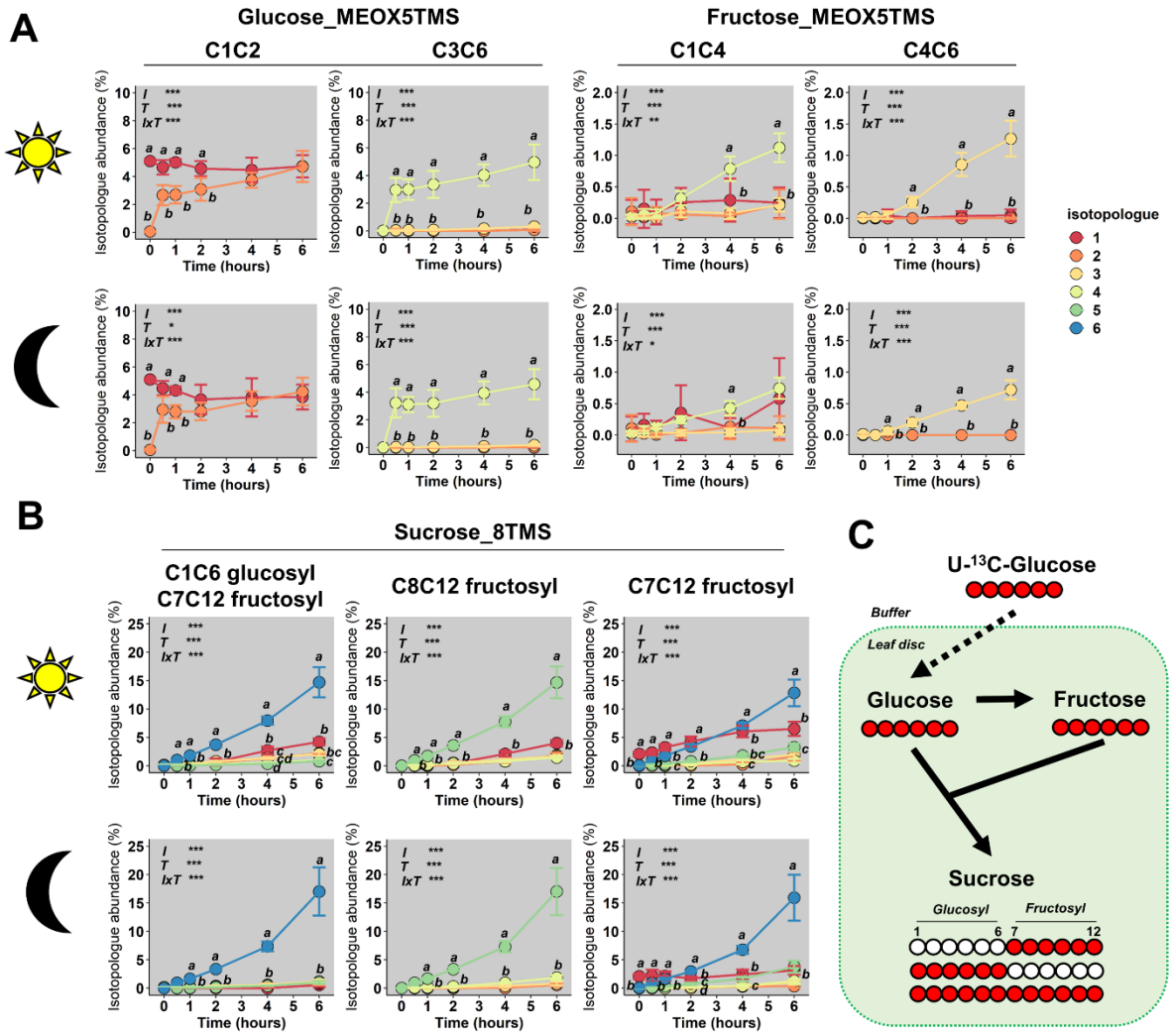

Figure 3. Carbon isotopologue distribution for glucose, fructose and sucrose in *B. napus* leaf discs fed with 10 mM U-^{13}C-glucose for up to 6 h under light and dark conditions. Carbon Isotopologue distribution of GC-MS fragments of **(A)** glucose and fructose and **(B)** sucrose. **(C)** Metabolic map of carbon transitions supporting our results (red circles = ^{13}C atoms, white circles= ^{12}C atoms). The effect of the two factors ("isotopologue" (*I*) and "time" (*T*)) and their interactions (*IxT*) was assessed with a two-way ANOVA (ns: not significant; *, p-value<0.05; **, p-value<0.01; ***, p-value<0.001). When *I* and/or *IxT* effects were significant, statistical differences were assessed at each timepoint with a post-hoc Tukey HSD test (p-value < 0.05). Isotopologue groups that were significantly separated are indicated with different letters. The complete dataset is available in **Table S2**.

3.4. Light-dependent regulation of serine biosynthesis pathways introduced specific CIDs into serine fragments

The increase of mean ^{13}C-enrichment of serine fragments in the light was essentially driven by an increase in M1 isotopologues (**Figure 4A**). M2 isotopologues weakly increased during the time course but always remained lower than M1 isotopologues. Thus, the production of fully ^{13}C-labelled serine was relatively negligible. The M1 isotopologue of the Glycine_2TMS_C2 fragment was also significantly increased with time. These results reflect the commitment of decarboxylations ($^{13}CO_2$) to photorespiration through Rubsico reassimilation and the Calvin cycle [42, 64]. Among these ^{13}C-decarboxylations, the glucose-6-phosphate (G6P) shunt was not considered here because it would lead to an important production of fully ^{13}C-labeled serine [16] and this was not observed. Given the weak plastidial PDH flux compared to mitochondrial PDH [16, 23], only mitochondrial decarboxylations (PDH, TCA cycle enzymes) were considered (**Figure 4B**). Analysis of CID for serine and glycine revealed contrasted patterns between light and dark conditions. The M1 isotopologue of Glycine_3TMS_C2 was not significantly changed with time (in comparison to the zero-time point). Both M1 and M2 isotopologues of serine fragments were produced in relatively similar proportions (**Figure 4A**). Among known serine biosynthesis pathways, the phosphorylated and the glycerate pathways can both produce serine under non-photorespiratory conditions by using glycolytic 3-phosphoglycerate (3-PGA) [65]. Thus, fully ^{13}C-labelled serine may have been produced in the dark from glycolytic 3-PGA, leading to an increase of M2 isotopologues for the C1C2 and C2C3 fragments of serine (**Figure 4C**). Dark production of M1 isotopologues of serine is more difficult to explain. However, the oxidative branch of the pentose phosphate pathway has a higher activity in the dark compared to light conditions [66, 67]. By combining oxidative and non-oxidative branches of this pathway, fructose-6-phosphate molecules (F6P) labelled on C1-C2 or C3-C6 carbons could be made from ^{13}C-labelled sugars (interactions with ^{12}C pools). Then, the commitment of such F6P molecules to glycolysis could produce 3-PGA labelled on either the C3 or C1C2 carbons, thereby explaining the occurrence of an M1 isotopologue of the Serine_3TMS_C2C3 fragment. Overall, these isotopic patterns infer contributions from multiple metabolic pathways to the biosynthesis of serine according to light availability.

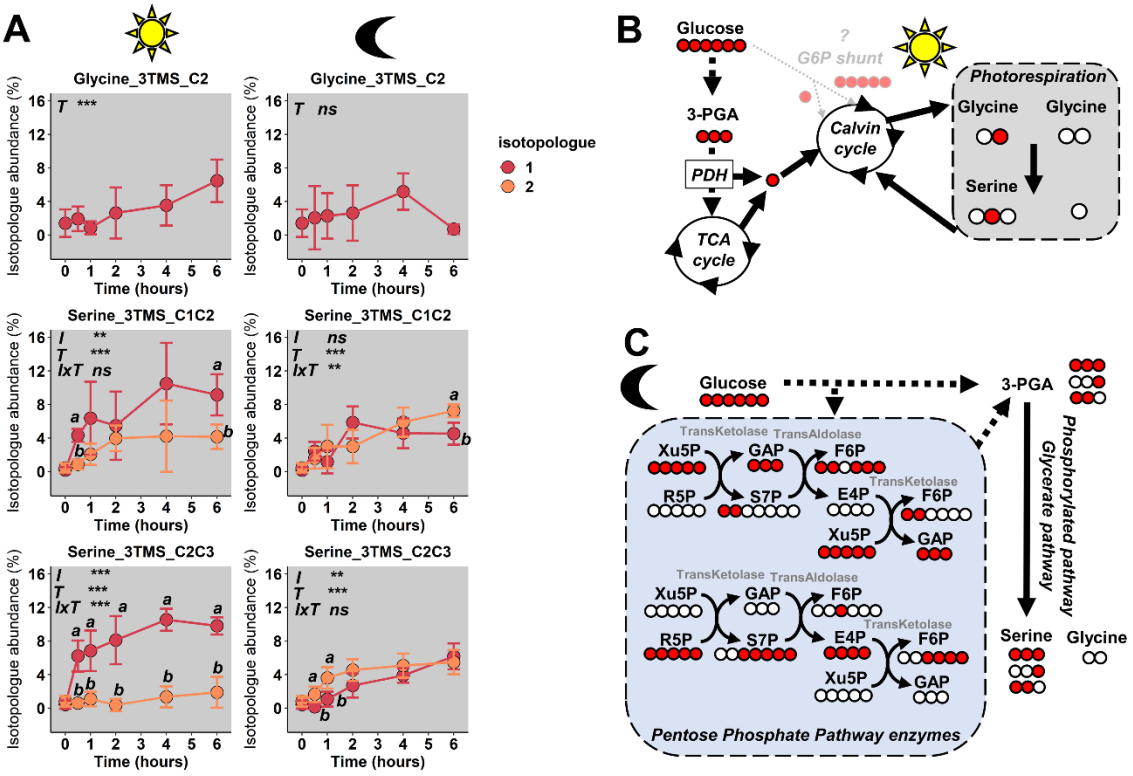

Figure 4. Carbon isotopologue distribution for glycine and serine from *B. napus* leaf discs fed with 10 mM U-^{13}C-glucose for up to 6 h under light and dark conditions. (**A**) Carbon Isotopologue distribution for glycine and serine fragments. (**B**) and (**C**) Metabolic maps of carbon transitions supporting our results in light and dark conditions (red circles = ^{13}C atoms, white circles = ^{12}C atoms). Direct contribution of G6P shunt to serine biosynthesis through the Calvin cycle was not observed in light conditions because the production of fully ^{13}C-labeled serine was negligible. Plastidial PDH was not considered due to its low flux compared to mitochondrial PDH in light conditions [16, 23]. Red circles = ^{13}C atoms, white circles= ^{12}C atoms. The effect of the two factors ("isotopologue" (*I*) and "time" (*T*)) and their interactions (*IxT*) was assessed with a two-way ANOVA (ns: not significant; *, p-value<0.05; **, p-value<0.01; ***, p-value<0.001). When *I* and/or *IxT* effects were significant, statistical differences were assessed at each timepoint with a post-hoc Tukey HSD test (p-value < 0.05). Isotopologue groups that were significantly separated are indicated with different letters. The complete dataset in available in **Table S2**.

3.5. Decarboxylations from mitochondrial PDH and the TCA cycle in the light are rapidly reallocated to TCA cycle by the Calvin cycle, photorespiration and glycolysis

Given the low accuracy of the Pyruvate_MEOXTMS_C1C3 fragment at low ^{13}C enrichments (see timepoint 0), we used the fragment Alphaalanine_2TMS_C2C3 as a proxy accurately evaluate ^{13}C-labelling of pyruvate (**Figure 5A**). Both M1 and M2 isotopologues of alpha-alanine increased significantly during the time course and suggested that pyruvate was labelled at C2-C3 positions and only labelled at either C2 or C3 (**Figure 5B**). Interestingly, the contribution of U-^{13}C-glucose and light-produced ^{13}C-serine could lead to this pattern in Alphaalanine_2TMS_C2C3. Analysis of glutamate and succinate also revealed an important increase of both M1 and M2 isotopologues (**Figure 5A**). Their M3 and M4 isotopologues were always lower than their M1 and M2 isotopologues and remained rather affected over time. Overall, these fragments mirrored the CID of 2-oxoglutarate. Given the large biological variability and the weak isotopologue abundances observed, citrate fragments were discarded from the analysis. To evaluate the metabolic origin of the M1 isotopologue in succinate and glutamate fragments, a survey of carbon atom transitions was performed using as inputs U-^{13}C-glucose (red circles), photorespiratory ^{13}C-serine (blue circle), and their respective ^{12}C-pools (white circles, M0 isotopologue) (**Figure 5B**). The contribution of PEPc and a first turn of the TCA cycle were considered for the biosynthesis of glutamate, succinate and malate. Interestingly, our analysis showed that the occurrence of M1 isotopologues was only explained by the commitment of photorespiratory ^{13}C-serine to the TCA cycle (blue circles). Indeed, in the absence of $^{13}CO_2$ refixed by the Calvin cycle, M1 and M3 isotopologues for glutamate and succinate cannot be produced by the first turn of the TCA cycle (**Figure S6**). Overall, our results suggested that ^{13}C from mitochondrial PDH and TCA cycle decarboxylations were reallocated to the TCA cycle by photorespiration and glycolysis in *B. napus* leaves. CID analysis for the Malate_3TMS_C1C4 fragment revealed a higher increase of M1 isotopologue compared to M2 isotopologue but also a significant increase of M3 isotopologue during the time course (**Figure 5A**). Here, the abundance of M2 isotopologue was relatively similar in both malate and glutamate fragments. Thus, the higher level of M1 and M3 isotopologues in malate probably reflected the additional contribution of PEPc activity. A detailed analysis of M3 isotopologues showed that PEPc contributed to nearly 75% for the production of this isotopologue compared to 25% by the TCA cycle (**Figure S7A**). In the metabolic map, M1 isotopologue of malate could be produced by the fixation of $H^{12}CO_3^-$ on photorespiratory-derived ^{13}C backbones or the fixation of $H^{13}CO_3^-$ on ^{12}C backbones. Here, leaf discs were in a $^{12}CO_2$ atmosphere during the experiment and their photosynthetic activity would favour the decarboxylation of $^{12}CO_2$ by photorespiration (GDC) Hence, the M1 isotopologue of malate also reflected the commitment of photorespiratory ^{13}C-serine (blue circles), as for glutamate and succinate (**Figure 5B**).

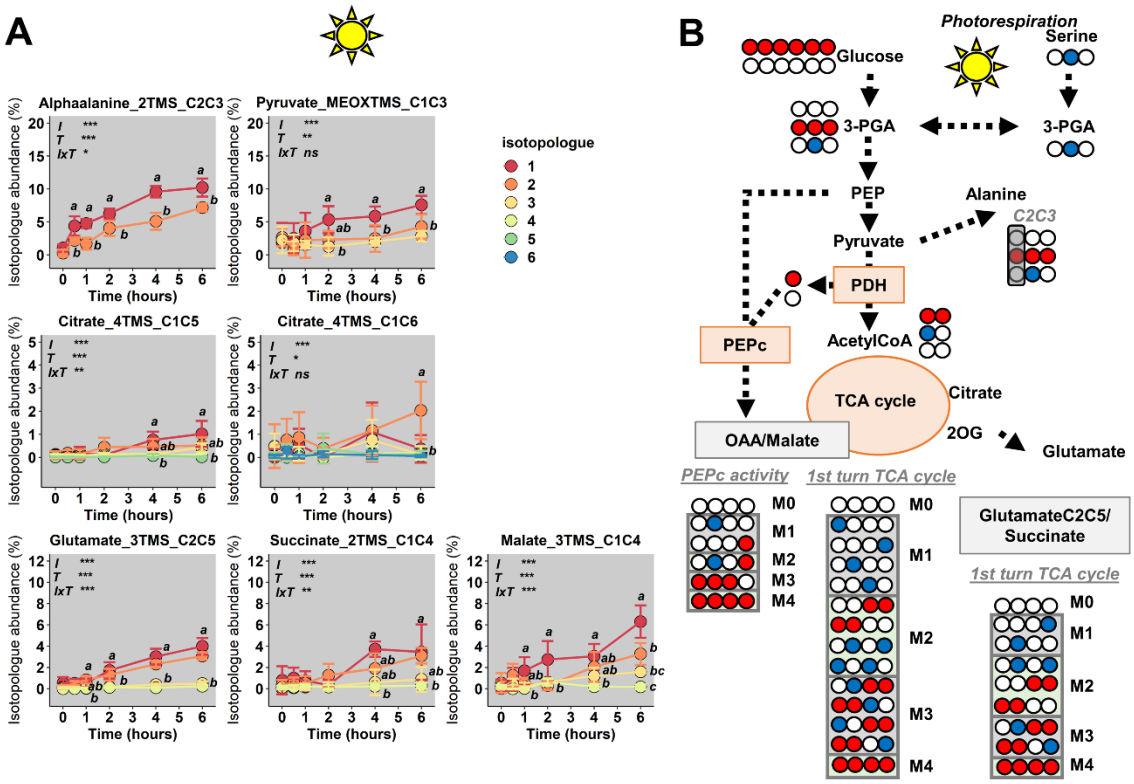

Figure 5. Carbon isotopologue distribution for TCA cycle derived metabolites from *B. napus* leaf discs fed with 10 mM U-^{13}C-glucose for up to 6 h under light conditions. (A) Carbon isotopologue distribution for alpha-alanine, pyruvate, citrate, succinate, glutamate and malate fragments. **(B)** Metabolic map of carbon transitions supporting our results (red circles = ^{13}C atoms from U-^{13}C-glucose, blue circles = ^{13}C atoms from photorespiratory-derived ^{13}C-serine, white circles = ^{12}C atoms). The metabolic map considered the contribution of glucose and photorespiratory-derived serine to the biosynthesis of glycolytic metabolites. For TCA cycle intermediates, we considered the contribution of PEPc and a first turn of the TCA cycle to the biosynthesis of glutamate, succinate and malate. The effect of the two factors ("isotopologue" (*I*) and "time" (*T*)) and their interactions (*IxT*) was assessed with a two-way ANOVA (ns: not significant; *, p-value<0.05; **, p-value<0.01; ***, p-value<0.001). When *I* and/or *IxT* effects were significant, statistical differences were assessed at each timepoint with a post-hoc Tukey HSD test (p-value < 0.05). Isotopologue groups that were significantly separated are indicated with different letters. The complete dataset in available in **Table S2**.

3.6. Contribution of glycolysis and the pentose phosphate pathway to fuel the TCA cycle in the dark

Analysis of CID in dark conditions revealed a dominant and significant increase of M2 isotopologues compared to light conditions for the following fragments: Alphaalanine_2TMS_C2C3, Citrate_4TMS_C1C5, Glutamate_3TMS_C2C5 and Succinate_2TMS_C1C4 (**Figures 5A, 6A**). Since these M2 isotopologues can come from U-^{13}C-glucose catabolism (**Figure S6**), these results confirmed a major contribution of glycolysis to TCA cycle activity in the dark (**Figure 2**). Besides this, a significant increase of M1, M3 and M4 isotopologues was also observed for all of these fragments. M3 and M4 isotopologues of glutamate and succinate fragments corresponded to the combined contribution of PEPc ^{13}C-refixation and the TCA cycle and showed higher levels in the dark than in the light (**Figures 5A, 6A, S6**). These results suggested a higher rate for TCA cycle activity in the dark than in the light. Given the isotopic profile of serine in the dark (**Figure 4C**), a survey of carbon atom transitions was performed using as inputs U-^{13}C-glucose (red circles), ^{13}C-3PGA derived from pentose phosphate pathway enzymes (blue circle), and their respective ^{12}C-pools (white circles, M0 isotopologue) (**Figure 6B**). The analysis showed that M1 isotopologues in glutamate and succinate fragments could be due to ^{13}C-3PGA derived from pentose phosphate pathway enzymes. CID analysis for the Malate_3TMS_C1C4 fragment revealed a similar increase of M1, M2 and M3 isotopologues along the studied time course (no statistical differences between them) while the M4 isotopologue increased more slowly (**Figure 6A**). This pattern strongly differed from glutamate CID, notably for the M3 isotopologue. Specific analysis of the M3 isotopologue suggested that PEPc activity had a higher contribution to this isotopologue in the dark compared to the TCA cycle (75% versus 25%, **Figure S7B**). Similar to light conditions, PEPc activity in a $^{12}CO_2$ atmosphere probably preferentially fixed ^{12}C at the C4 position of malate. Thus, the M1 isotopologue of malate in dark conditions could reflect the commitment of ^{13}C-PGA derived from pentose phosphate pathway enzymes (**Figure 6B**). Overall, these results highlighted the higher contribution of glycolysis to the TCA cycle in dark conditions compared to light conditions. The pentose phosphate pathway could also contribute to TCA cycle activity in the dark.

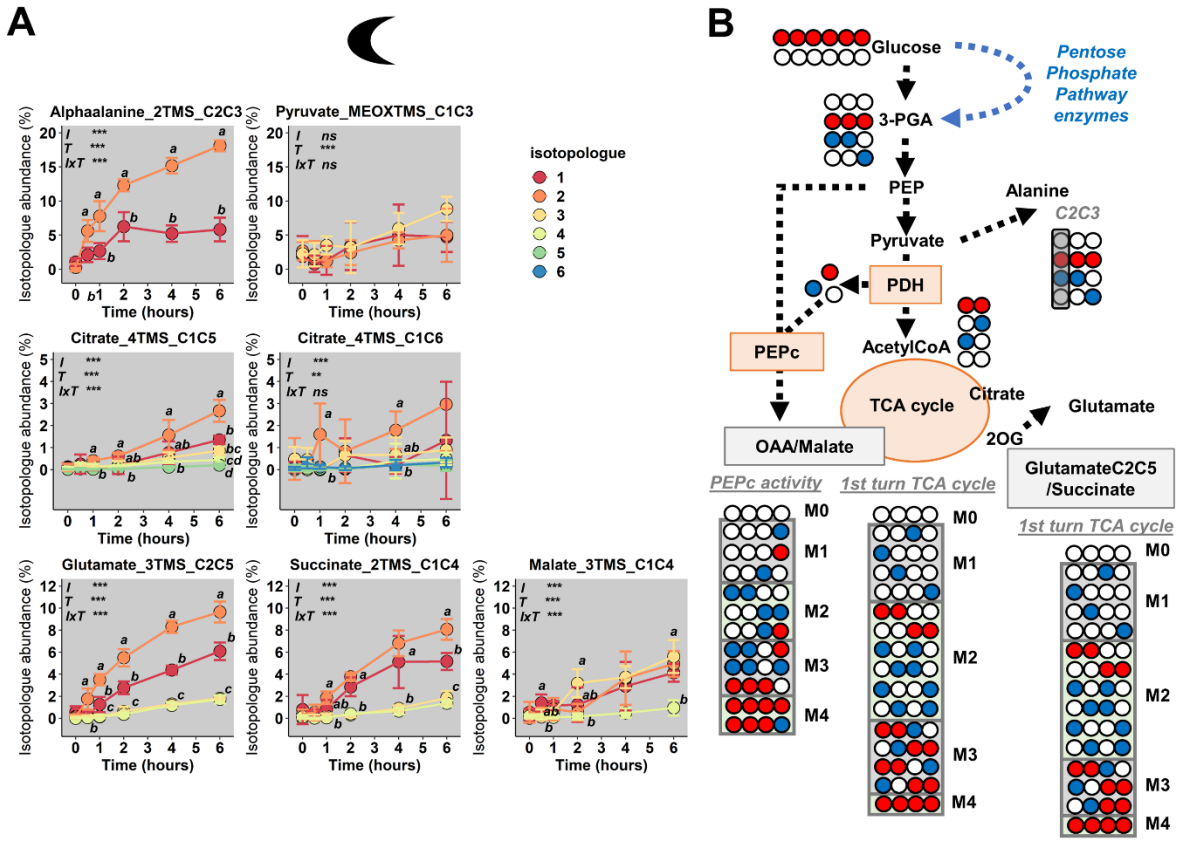

Figure 6. Carbon isotopologue distribution for TCA cycle derived metabolites from *B. napus* leaf discs fed with 10 mM U-^{13}C-glucose for up to 6 h under dark conditions. (A) Carbon isotopologue distribution for alpha-alanine, pyruvate, citrate, succinate, glutamate and malate fragments. **(B)** Metabolic map of carbon transitions supporting our results (red circles = ^{13}C atoms from U-^{13}C-glucose, blue circles = ^{13}C atoms derived from pentose phosphate pathway enzymes, white circles = ^{12}C atoms). The metabolic map considered the contribution of glucose and pentose phosphate pathway enzymes to the biosynthesis of glycolytic metabolites. For TCA cycle intermediates, we considered the contribution of PEPc and a first turn of the TCA cycle to the biosynthesis of glutamate, succinate and malate. The effect of the two factors ("isotopologue" (*I*) and "time" (*T*)) and their interactions (*IxT*) was assessed with a two-way ANOVA (ns: not significant; *, p-value<0.05; **, p-value<0.01; ***, p-value<0.001). When *I* and/or *IxT* effects were significant, statistical differences were assessed at each timepoint with a post-hoc Tukey HSD test (p-value < 0.05). Isotopologue groups that were significantly separated are indicated with different letters. The complete dataset in available in **Table S2**.

4. Discussion

Central carbon metabolism is an important target to consider for future crop improvement in a changing climate context [68]. Recent developments of ^{13}C-based tracing and modelling approaches to study plant metabolism have paved the way for a better integration of metabolic regulations within complex plant primary metabolism networks [22, 69, 70]. That said, the use of targeted approaches with ^{13}C-metabolic probes has been deployed only to a limited extent on crops. This experimental strategy could help identify the topology of carbon allocation processes within central metabolism of crop plant leaves as a function of fluctuating environmental conditions such as light availability.

Here, we validated a leaf disc method and U-^{13}C-glucose incorporation to decipher carbon allocation processes in source leaves of *B. napus* with respect to light versus dark. Overall, the introduction of glucose into leaf discs during a 6 h time course period did not impact net CO_2 assimilation in the light and respiration in the dark (**Figure 1**). In other leaf disc experiments with Arabidopsis, incubations with different exogenous metabolites (sugars, glycolytic intermediates, organic acids and amino acids) at 10 mM concentrations in dark conditions did not significantly increase respiratory rates after 6 h, except for 3-PGA [71, 72]. Given that some of these compounds were highly accumulated in leaf discs only after 4 h [72], the physiological response of leaf discs to exogenous metabolites may require several hours to be effective. Indeed, glucose was not significantly accumulated after 4 h in [72], in agreement with our observations after 6 h (**Figure 1**). Non-aqueous fractionation experiments using Arabidopsis showed that nearly 60% of glucose was located to the vacuole [18, 73, 74]. Again, in source leaves of tomato, up to 90% of glucose was found in the vacuole [75]. A recent ^{13}C-metabolic flux analysis showed that vacuolar sugar pools are largely inactive in light conditions. Thus, a large amount of metabolically inactive glucose in our experiment could restrict U-^{13}C-glucose uptake and could also dilute the measurement of U-^{13}C-glucose taken up by leaf discs [76]. As a consequence, ^{13}C-enrichment for glucose could be lower than for other metabolites. Here, mean ^{13}C-enrichment for glucose and fructose, the metabolic precursors of sucrose, was relatively low compared to sucrose. Thus, the presence of a large amount of metabolically inactive glucose contributed to maintain glucose levels at physiological concentrations during the kinetic time course.

Overall, the experimental setup proposed allowed us to investigate the response of central carbon metabolism of *B. napus* leaves to light availability in physiologically reliable conditions. At similar ^{13}C-enrichments for glucose, fructose and sucrose in light and dark conditions, a reduced commitment of ^{13}C carbons towards pyruvate was observed in the light combined with a reduced TCA cycle activity, as judged by the differences of mean ^{13}C enrichments in TCA cycle intermediates between light and dark conditions (**Figures 2, 4, 6**). Previous studies suggested that some thioredoxins (TRX) are involved in the inhibition of TCA cycle activity in the light in Arabidopsis [29, 33, 37]. However, the regulation mediated by TRXo1 and TRXh2 was independent from light conditions and its associated glycolytic regulation [41]. Recently, two mitochondrial phosphatases were identified as key regulators of some TCA cycle enzyme activities [37]. However, a comparison between U-^{13}C-pyruvate

and U-^{13}C-glucose labelling suggested that they acted independently of glycolysis. Therefore, a reduced glycolytic flux in the light when compared to the dark could actively participate to the observed lower TCA cycle activity in the light. Three pyruvate-supplying pathways sustaining respiratory metabolism have been identified: The transport of pyruvate, the transport of alanine and the transport malate (derived from PEP) [30, 31, 77]. When one of the transport pathways was blocked, the activity of the remaining pathways maintained mitochondrial TCA cycle activity. Thus, suggesting that the restriction of TCA cycle activity in the light would require all three pathways to be down-regulated. Here, we observed a significant reduction of ^{13}C-enrichments in pyruvate, alanine and malate under light conditions compared to dark conditions. These results confirmed that glycolysis strongly controlled the availability of these respiratory substrates for TCA cycle activity. In previous experiments with *B. napus* leaf discs, incorporation of U-^{13}C-pyruvate did not identify a significant reduction of mean ^{13}C-enrichment in TCA cycle intermediates [42]. In other words, bypassing glycolysis in *B. napus* leaf discs completely suppressed the inhibition of TCA cycle activity in the light. Therefore, our ^{13}C-labelling experiments showed that glycolysis was the major pathway regulating TCA cycle inhibition in the light in *B. napus* source leaves (**Figure 7**).

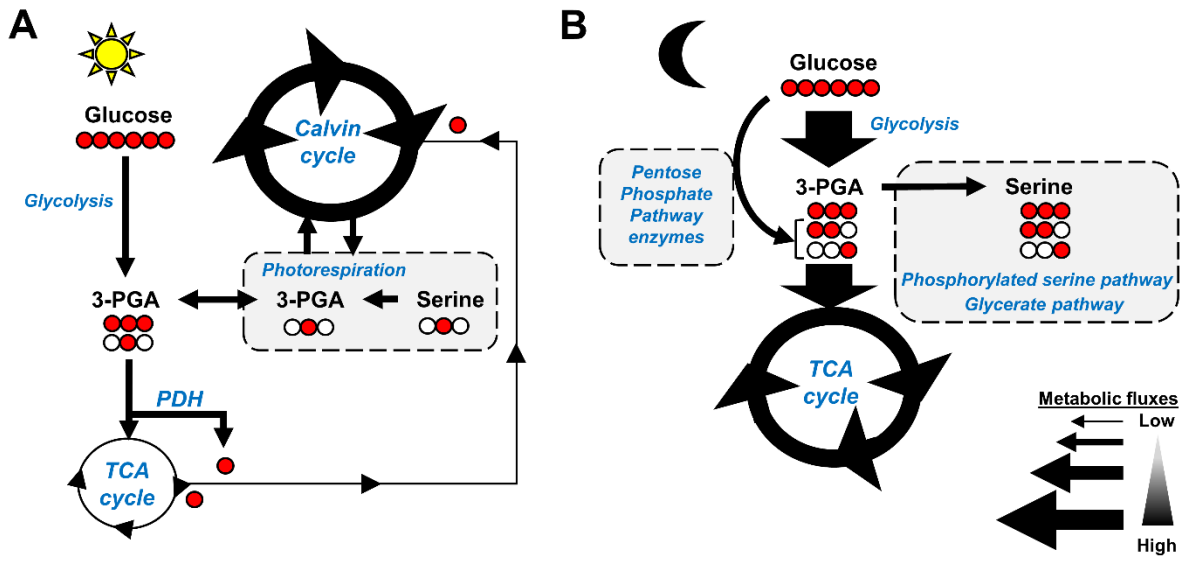

Figure 7. Proposed flux modes in *B. napus* source leaves during U-^{13}C-glucose incorporation in light and dark conditions. (**A**) Light and (**B**) dark conditions. Glycolysis is inhibited in the light and constrains TCA cycle activity by restricting the availability of major respiratory substrates. Mitochondrial decarboxylations (TCA cycle and PDH) rather than from the G6P shunt are actively assimilated by photosynthesis, leading to the reallocation of some photorespiratory carbon backbones towards the TCA cycle. Both glycolysis and the pentose phosphate pathway could be involved in the biosynthesis of serine in the dark and in the TCA cycle activity in the dark. Thicker arrows correspond to higher metabolic fluxes.

By combining CID measurements and analysis of carbon transitions in plant metabolic networks, we provided isotopic evidence for the light/dark modulation of serine biosynthesis pathways (**Figure 4**). Notably, our results supported the reassimilation of ^{13}C-labelled decarboxylations by the Calvin cycle rather than a direct contribution from U-^{13}C-glucose. A recent U-^{13}C-glucose incorporation in Arabidopsis also identified ^{13}C-redistribution towards serine, but isotopic data did not confirm or rule out the contribution of the G6P shunt [78]. Here, M2 isotopologue for Serine_3TMS fragments remained weakly labelled or unlabelled during the time course. If ribulose-5-phosphate, the product of the G6P shunt, was committed to the Calvin cycle, then a significant increase would be expected for this labelling pattern [66]. Thus, the observed labelling pattern could have reflected the specific use of plastidial G6P for this shunt. The transport of G6P into plastids is essential for the G6P shunt in non-photosynthetic tissues [79, 80]. Plastidial G6P dehydrogenases can retain a significant activity in illuminated leaves to allow flux through the G6P shunt [67]. Here, the presence of an important photosynthetic activity (**Figure 1**) in a $^{12}CO_2$ atmosphere is expected to produce poorly ^{13}C-labelled plastidial G6P in the light, even when considering the reassimilation of ^{13}C-labelled decarboxylations. However, a recent ^{13}C-MFA proposed that this shunt operated with cytosolic G6P and partially used ^{12}C-sugars from the vacuole [28]. Another explanation for the low presence of M2 isotopologue Serine_3TMS fragments could be the weak flux of the G6P shunt compared to RuBiSCO activities: 20-fold lower for carboxylation, 8-fold lower for oxygenation [16, 28]. Nevertheless, decarboxylations from the G6P shunt can represent up to 90% of decarboxylations in the light compared to only 10% for TCA cycle enzymes [28]. In others words, the G6P shunt could still contribute to the ^{13}C-labelling of serine in the light (M1 isotopologue) through the production of $^{13}CO_2$. In fact, a metabolic flux analysis (MFA) showed that mitochondrial TCA cycle enzymes, the G6P shunt and plastidial PDH are the major contributors of CO_2 production in plant cell cultures [81]. However, two ^{13}C-MFA showed that plastidial PDH had a negligible flux compared to mitochondrial PDH in illuminated leaves [16, 23]. In previous experiments, we observed the appearance of the same labelling pattern at equivalent speeds and isotopic enrichments for glycine and serine when performing U-^{13}C-pyruvate incorporations [42]. Given that gluconeogenesis is not observed with U-^{13}C-pyruvate, the contribution of the G6P shunt to the ^{13}C-labelling of serine during U-^{13}C-glucose incorporation in the light can be questioned. Overall, our results provided additional isotopic evidences for the reassimilation of mitochondrial decarboxylations from PDH and the TCA cycle by the Calvin cycle, leading to a rapid labelling of photorespiratory intermediates (**Figure 7A**). So, the reassimilation of respiratory CO_2 could have an important contribution to the final plant net carbon balance under environmental conditions affecting stomatal aperture [15].Indeed, most of the synthetic biochemical bypasses for photorespiration are based on the reassimilation of CO_2 produced from chloroplast glycolate catabolism [82, 83]. The use of ^{13}C-metabolic probes (U-^{13}C-glucose, U-^{13}C-pyruvate) to evaluate the reassimilation of CO_2 respiratory losses will be highly relevant for future crop improvement.

Regarding serine biosynthesis in the dark, we identified the contribution of glycolysis-derived pathways for the production of M2 isotopologues (**Figure 4**). Since multiple steps of glycolysis can work both in the cytosol and in plastids, both the plastidial phosphorylated

serine pathway and the cytosolic glycerate pathway could be involved [65, 84, 85]. Arabidopsis mutant analysis for the phosphorylated serine pathway confirmed its preponderant role for serine biosynthesis in non-photorespiratory conditions and in non-photosynthetic tissues [86-89]. However, the importance of the glycerate pathway has not yet been studied in detail, notably for dark conditions in C_3 plants [90]. Thus, the specific contribution of each pathway will strongly depend on the transport of ^{13}C-labelled glycolytic intermediates between cytosol and plastids. Here, the occurrence of M1 isotopologue of serine fragments in the dark suggests the contribution of pentose phosphate pathway enzymes using both ^{13}C and ^{12}C-labelled sugar pools (**Figure 4C**). Since both photosynthesis and photorespiration are not active in the dark, it is likely that the direct contribution of U-^{13}C-glucose to the activity of the pentose phosphate pathway was more pronounced and easily visible on serine fragments compared to light conditions. Total G6P dehydrogenase activity is much higher in leaves subjected to dark conditions compared to light conditions [67]. However, the activation of starch degradation in the dark could also produce ^{12}C-glucose for this pathway. The plants used here received 4 h of light before the beginning of the kinetic time course, which could produce a substantial amount of starch to remobilize. The transport of ^{13}C-labelled G6P from cytosol to plastids needs to be tested in the dark to further validate the pentose phosphate pathway hypothesis. The rate of this transport will also help to separate the respective contribution of the phosphorylated serine pathway and the glycerate pathway to serine biosynthesis (**Figure 7B**). The other hypothesis to explain the presence of M1 isotopologue of serine fragments in the dark could be the activation of gluconeogenesis. $H^{13}CO_3^-$ labelling experiments in dark conditions showed that gluconeogenesis could operate from TCA cycle intermediates, leading to the labelling of carbon atoms 3 and 4 of glucose [34, 39]. However, only the M4 isotopologue of Glucose_MEOX5TMS_C3C6 fragment increased in the dark. Thus, gluconeogenesis from TCA cycle intermediates was either inactive or negligible during the labelling time course.

Our results also showed that ^{13}C-labelled carbon backbones from photorespiratory intermediates were actively committed to the TCA cycle in the light, producing the M1 isotopologue in both Glutamate_3TMS_C2C5 and Succinate_2TMS_C1C4 fragments (**Figure 5**). Since such ^{13}C-labelled photorespiratory intermediates appeared to come from mitochondrial decarboxylations, our results provide isotopic evidences for an active metabolic connection between the TCA cycle, glycolysis and photorespiration in the light (**Figure 7A**). Previous isotopic studies confirmed that photorespiratory glycine was more committed to organic acid biosynthesis, possibly via glycolysis and the TCA cycle, rather than to gluconeogenesis[62, 78]. Recently, an important molecular connection between chloroplasts and mitochondria has been shown in Arabidopsis and supported their physical interaction *in vivo* [91]. Multiple glycolytic enzymes (phosphoglycerate mutase, enolase, pyruvate kinase) can form a glycolytic complex *in vivo* (metabolon) with a chloroplast triose phosphate translocator and a mitochondrial voltage-dependent anion channel [91]. This could facilitate an efficient substrate channelling of 3-PGA and 2-PGA towards pyruvate. Since photorespiratory 3-PGA is produced in chloroplasts [92], the functioning of this metabolon could contribute to the production of M1 isotopologue of succinate and glutamate fragments in our study. Overall, our ^{13}C-labelling experiments strongly support

active metabolic interactions between chloroplastic and mitochondrial metabolisms in the light (**Figure 7A**).

5. Conclusions

In this study, the effect of light and dark on central carbon metabolism was studied in *B. napus* source leaf discs using gas-exchange measurements and U-^{13}C-glucose incorporation. Overall, our results suggested that: i) Leaf discs are a relevant material to explore short-term changes in plant metabolism; ii) glycolysis is the major pathway involved in the inhibition of the TCA cycle in the light by controlling the availability of respiratory substrates, iii) mitochondrial decarboxylations from PDH and the TCA cycle are actively reintroduced back into the TCA cycle by the concerted action of photosynthesis, photorespiration and glycolysis. As recently shown with the glycolytic metabolon linking chloroplasts to mitochondria for rapid channelling of 3-PGA [91], the metabolic connections between chloroplasts, mitochondria and peroxisomes appear to be an important gap to be filled in the future.

Supplementary Materials: Figure S1: Experimental setup used to measure leaf disc gas exchanges; **Figure S2**: Relative contribution of glucosyl and fructosyl moieties of Sucrose_8TMS to *m/z* 341, 437 and 451**; Figure S3:** Isotopic pollution of the Glucose_MEOX5TMS_C1C2 fragment by C3-C4-C5-C6 carbons of glucose (fragment m/z 157); **Figure S4:** Mathematical framework for the correction of isotopic pollution from Glucose_MEOX5TMS_C3C6 fragment (m/z 157) on Glucose_MEOX5TMS_C1C2 fragment (m/z 160); **Figure S5:** Relative metabolite levels of *B. napus* leaf discs fed with 10 mM U-^{13}C-glucose for up to 6 h under either light or dark conditions; **Figure S6:** Impact of the "no $^{13}CO_2$ refixation by the Calvin cycle" hypothesis on isotopologue detection of glutamate, succinate and malate fragments; **Figure S7:** Detailed analysis of M3 isotopologues of glutamate, succinate and malate fragments from *B. napus* leaf discs fed with 10 mM U-^{13}C-glucose for up to 6 h under light conditions; **Table S1**: Elution times of the standards with the GC-MS analytical method; **Table S2** : Complete isotopic dataset, **Example file**: GC-MS output file containing the names of metabolites used for Galaxy-based processing.

Contributions: Conceptualization, Y.D. and A.B.; methodology, Y.D. and S.B; software, Y.D.; validation, Y.D., S.B.; formal analysis, Y.D.; investigation, Y.D. and A.B.; data curation, Y.D., S.B.; writing—original draft preparation, Y.D.; writing—review and editing, Y.D. and A.B.; visualization, Y.D.; supervision, Y.D.; project administration, Y.D.; funding acquisition, Y.D. All authors have read and agreed to the published version of the manuscript.

Funding: This research was supported by the IB2021_TRICYCLE project funded by the INRAE BAP division and by the METABOHUB project funded by the program Investments for the Future of the French National Agency for Research (ANR grant number 11-INBS-0010).

Data Availability Statement: The original contributions presented in the study are included in the article/supplementary material.

Acknowledgments: P2M2 (Metabolic Profiling & Metabolomics Platform, Le Rheu, France, https://p2m2.hub.inrae.fr/) and its staff members are gratefully acknowledged for access to mass spectrometry facilities. We would like to thank Michael Hodges for carefully reading the manuscript.

References:

[1] H.A. Maeda, A.R. Fernie, Evolutionary History of Plant Metabolism, Annu Rev Plant Biol, 72 (2021) 185-216.
[2] L.J. Sweetlove, K.F. Beard, A. Nunes-Nesi, A.R. Fernie, R.G. Ratcliffe, Not just a circle: flux modes in the plant TCA cycle, Trends Plant Sci, 15 (2010) 462-470.
[3] S. Timm, M. Hagemann, Photorespiration - how is it regulated and regulates overall plant metabolism?, J Exp Bot, (2020).
[4] H. Treves, A. Kuken, S. Arrivault, H. Ishihara, I. Hoppe, A. Erban, M. Hohne, T.A. Moraes, J. Kopka, J. Szymanski, Z. Nikoloski, M. Stitt, Carbon flux through photosynthesis and central carbon metabolism show distinct patterns between algae, C3 and C4 plants, Nat Plants, 8 (2022) 78-91.
[5] A.R. Fernie, C.W.B. Bachem, Y. Helariutta, H.E. Neuhaus, S. Prat, Y.L. Ruan, M. Stitt, L.J. Sweetlove, M. Tegeder, V. Wahl, S. Sonnewald, U. Sonnewald, Synchronization of developmental, molecular and metabolic aspects of source-sink interactions, Nat Plants, 6 (2020) 55-66.
[6] M.E. Dusenge, A.G. Duarte, D.A. Way, Plant carbon metabolism and climate change: elevated CO2 and temperature impacts on photosynthesis, photorespiration and respiration, New Phytol, 221 (2019) 32-49.
[7] F. Flugel, S. Timm, S. Arrivault, A. Florian, M. Stitt, A.R. Fernie, H. Bauwe, The Photorespiratory Metabolite 2-Phosphoglycolate Regulates Photosynthesis and Starch Accumulation in Arabidopsis, Plant Cell, 29 (2017) 2537-2551.
[8] A.J. Simkin, P.E. Lopez-Calcagno, P.A. Davey, L.R. Headland, T. Lawson, S. Timm, H. Bauwe, C.A. Raines, Simultaneous stimulation of sedoheptulose 1,7-bisphosphatase, fructose 1,6-bisphophate aldolase and the photorespiratory glycine decarboxylase-H protein increases CO2 assimilation, vegetative biomass and seed yield in Arabidopsis, Plant Biotechnol J, 15 (2017) 805-816.
[9] S. Timm, M. Wittmiss, S. Gamlien, R. Ewald, A. Florian, M. Frank, M. Wirtz, R. Hell, A.R. Fernie, H. Bauwe, Mitochondrial Dihydrolipoyl Dehydrogenase Activity Shapes Photosynthesis and Photorespiration of Arabidopsis thaliana, Plant Cell, 27 (2015) 1968-1984.
[10] J.S. Amthor, A. Bar-Even, A.D. Hanson, A.H. Millar, M. Stitt, L.J. Sweetlove, S.D. Tyerman, Engineering Strategies to Boost Crop Productivity by Cutting Respiratory Carbon Loss, Plant Cell, 31 (2019) 297-314.
[11] L.J. Sweetlove, J. Nielsen, A.R. Fernie, Engineering central metabolism - a grand challenge for plant biologists, Plant J, 90 (2017) 749-763.
[12] A.R. Fernie, M. Stitt, On the discordance of metabolomics with proteomics and transcriptomics: coping with increasing complexity in logic, chemistry, and network interactions scientific correspondence, Plant Physiol, 158 (2012) 1139-1145.
[13] Y. Dellero, M. Heuillet, N. Marnet, F. Bellvert, P. Millard, A. Bouchereau, Sink/Source Balance of Leaves Influences Amino Acid Pools and Their Associated Metabolic Fluxes in Winter Oilseed Rape (Brassica napus L.), Metabolites, 10 (2020) 16.
[14] Y. Dellero, V. Clouet, N. Marnet, A. Pellizzaro, S. Dechaumet, M.F. Niogret, A. Bouchereau, Leaf status and environmental signals jointly regulate proline metabolism in winter oilseed rape, J Exp Bot, 71 (2020) 2098-2111.
[15] G. Tcherkez, P. Gauthier, T.N. Buckley, F.A. Busch, M.M. Barbour, D. Bruhn, M.A. Heskel, X.Y. Gong, K.Y. Crous, K. Griffin, D. Way, M. Turnbull, M.A. Adams, O.K. Atkin, G.D. Farquhar, G. Cornic, Leaf day respiration: low CO2 flux but high significance for metabolism and carbon balance, New Phytol, 216 (2017) 986-1001.
[16] Y. Xu, X. Fu, T.D. Sharkey, Y. Shachar-Hill, B.J. Walker, The metabolic origins of non-photorespiratory CO2 release during photosynthesis: A metabolic flux analysis, Plant Physiol, (2021).

[17] D.M. Daloso, D.B. Medeiros, L. Dos Anjos, T. Yoshida, W.L. Araujo, A.R. Fernie, Metabolism within the specialized guard cells of plants, New Phytol, 216 (2017) 1018-1033.
[18] M. Szecowka, R. Heise, T. Tohge, A. Nunes-Nesi, D. Vosloh, J. Huege, R. Feil, J. Lunn, Z. Nikoloski, M. Stitt, A.R. Fernie, S. Arrivault, Metabolic fluxes in an illuminated Arabidopsis rosette, Plant Cell, 25 (2013) 694-714.
[19] N.J. Kruger, S.K. Masakapalli, R.G. Ratcliffe, Assessing Metabolic Flux in Plants with Radiorespirometry, in: K. Jagadis Gupta (Ed.) Plant Respiration and Internal Oxygen: Methods and Protocols, Springer New York, New York, NY, 2017, pp. 1-16.
[20] R.G. Ratcliffe, Y. Shachar-Hill, Measuring multiple fluxes through plant metabolic networks, Plant J, 45 (2006) 490-511.
[21] H.K. Kotapati, P.D. Bates, 14C-Tracing of Lipid MetabolismLipid metabolism, in: D. Bartels, P. Dörmann (Eds.) Plant Lipids: Methods and Protocols, Springer US, New York, NY, 2021, pp. 59-80.
[22] S. Koley, K.L. Chu, T. Mukherjee, S.A. Morley, A. Klebanovych, K.J. Czymmek, D.K. Allen, Metabolic synergy in Camelina reproductive tissues for seed development, Science Advances, 8 (2022) eabo7683.
[23] K.L. Chu, S. Koley, L.M. Jenkins, S.R. Bailey, S. Kambhampati, K. Foley, J.J. Arp, S.A. Morley, K.J. Czymmek, P.D. Bates, D.K. Allen, Metabolic flux analysis of the non-transitory starch tradeoff for lipid production in mature tobacco leaves, Metab Eng, 69 (2022) 231-248.
[24] J.M. Buescher, M.R. Antoniewicz, L.G. Boros, S.C. Burgess, H. Brunengraber, C.B. Clish, R.J. DeBerardinis, O. Feron, C. Frezza, B. Ghesquiere, E. Gottlieb, K. Hiller, R.G. Jones, J.J. Kamphorst, R.G. Kibbey, A.C. Kimmelman, J.W. Locasale, S.Y. Lunt, O.D. Maddocks, C. Malloy, C.M. Metallo, E.J. Meuillet, J. Munger, K. Noh, J.D. Rabinowitz, M. Ralser, U. Sauer, G. Stephanopoulos, J. St-Pierre, D.A. Tennant, C. Wittmann, M.G. Vander Heiden, A. Vazquez, K. Vousden, J.D. Young, N. Zamboni, S.M. Fendt, A roadmap for interpreting (13)C metabolite labeling patterns from cells, Curr Opin Biotechnol, 34 (2015) 189-201.
[25] M.R. Antoniewicz, A guide to metabolic flux analysis in metabolic engineering: Methods, tools and applications, Metab Eng, 63 (2021) 2-12.
[26] T.J. Clark, L. Guo, J. Morgan, J. Schwender, Modeling Plant Metabolism: From Network Reconstruction to Mechanistic Models, Annu Rev Plant Biol, 71 (2020) 24.
[27] P.P. Gauthier, R. Bligny, E. Gout, A. Mahe, S. Nogues, M. Hodges, G.G. Tcherkez, In folio isotopic tracing demonstrates that nitrogen assimilation into glutamate is mostly independent from current CO2 assimilation in illuminated leaves of Brassica napus, New Phytol, 185 (2010) 988-999.
[28] Y. Xu, T. Wieloch, J.A.M. Kaste, Y. Shachar-Hill, T.D. Sharkey, Reimport of carbon from cytosolic and vacuolar sugar pools into the Calvin–Benson cycle explains photosynthesis labeling anomalies, Proceedings of the National Academy of Sciences, 119 (2022).
[29] P. da Fonseca-Pereira, P.V.L. Souza, A.R. Fernie, S. Timm, D.M. Daloso, W.L. Araujo, Thioredoxin-mediated regulation of (photo)respiration and central metabolism, J Exp Bot, 72 (2021) 5987-6002.
[30] X.H. Le, C.P. Lee, D. Monachello, A.H. Millar, Metabolic evidence for distinct pyruvate pools inside plant mitochondria, Nat Plants, (2022).
[31] X.H. Le, C.P. Lee, A.H. Millar, The mitochondrial pyruvate carrier (MPC) complex mediates one of three pyruvate-supplying pathways that sustain Arabidopsis respiratory metabolism, Plant Cell, 33 (2021) 2776-2793.
[32] C.P. Lee, M. Elsasser, P. Fuchs, R. Fenske, M. Schwarzlander, A.H. Millar, The versatility of plant organic acid metabolism in leaves is underpinned by mitochondrial malate-citrate exchange, Plant Cell, 33 (2021) 3700-3720.
[33] D.M. Daloso, K. Muller, T. Obata, A. Florian, T. Tohge, A. Bottcher, C. Riondet, L. Bariat, F. Carrari, A. Nunes Nesi, B.B. Buchanan, J.-P. Reichheld, W.L. Araujo, A.R. Fernie, Thioredoxin, a master regulator of the tricarboxylic acid cycle in plant mitochondria, Proc Natl Acad Sci U S A, (2015) 9.
[34] V.F. Lima, A. Erban, A.G. Daubermann, F.B.S. Freire, N.P. Porto, S.A. Candido-Sobrinho, D.B. Medeiros, M. Schwarzlander, A.R. Fernie, L. Dos Anjos, J. Kopka, D.M. Daloso, Establishment of a GC-MS-based (13) C-positional isotopomer approach suitable for investigating metabolic fluxes in plant primary metabolism, Plant J, 108 (2021) 21.

[35] A. Tovar-Mendez, J.A. Miernyk, D.D. Randall, Regulation of pyruvate dehydrogenase complex activity in plant cells, Eur J Biochem, 270 (2003) 1043-1049.
[36] G. Tcherkez, G. Cornic, R. Bligny, E. Gout, J. Ghashghaie, In vivo respiratory metabolism of illuminated leaves, Plant Physiol, 138 (2005) 1596-1606.
[37] Y. Zhang, J. Giese, S.M. Kerbler, B. Siemiatkowska, L. Perez de Souza, J. Alpers, D.B. Medeiros, D.K. Hincha, D.M. Daloso, M. Stitt, I. Finkemeier, A.R. Fernie, Two mitochondrial phosphatases, PP2c63 and Sal2, are required for posttranslational regulation of the TCA cycle in Arabidopsis, Mol Plant, 14 (2021) 1104-1118.
[38] D.B. Medeiros, L. Perez Souza, W.C. Antunes, W.L. Araujo, D.M. Daloso, A.R. Fernie, Sucrose breakdown within guard cells provides substrates for glycolysis and glutamine biosynthesis during light-induced stomatal opening, Plant J, 94 (2018) 583-594.
[39] D.M. Daloso, W.C. Antunes, D.P. Pinheiro, J.P. Waquim, W.L. Araujo, M.E. Loureiro, A.R. Fernie, T.C. Williams, Tobacco guard cells fix CO_2 by both Rubisco and PEPcase while sucrose acts as a substrate during light-induced stomatal opening, Plant Cell Environ, 38 (2015) 2353-2371.
[40] V.F. Lima, F.B.S. Freire, S.A. Cândido-Sobrinho, N.P. Porto, D.B. Medeiros, A. Erban, J. Kopka, M. Schwarzländer, A.R. Fernie, D.M. Daloso, Unveiling the dark side of guard cell metabolism, Plant Physiology and Biochemistry, 201 (2023) 107862.
[41] N.P. Porto, R.S.C. Bret, P.V.L. Souza, S.A. Candido-Sobrinho, D.B. Medeiros, A.R. Fernie, D.M. Daloso, Thioredoxins regulate the metabolic fluxes throughout the tricarboxylic acid cycle and associated pathways in a light-independent manner, Plant Physiol Biochem, 193 (2022) 36-49.
[42] Y. Dellero, S. Berardocco, C. Berges, O. Filangi, A. Bouchereau, Validation of carbon isotopologue distribution measurements by GC-MS and application to 13C-metabolic flux analysis of the tricarboxylic acid cycle in Brassica napus leaves, Front Plant Sci, 13 (2023) 22.
[43] J.D. Berrocoso, O.J. Rojas, Y. Liu, J. Shoulders, J.C. González-Vega, H.H. Stein, Energy concentration and amino acid digestibility in high-protein canola meal, conventional canola meal, and soybean meal fed to growing pigs, Journal of Animal Science, 93 (2015) 2208-2217.
[44] S.V. Hatzig, J.N. Nuppenau, R.J. Snowdon, S.V. Schiessl, Drought stress has transgenerational effects on seeds and seedlings in winter oilseed rape (Brassica napus L.), BMC Plant Biol, 18 (2018) 297.
[45] G.W. Rathke, O. Christen, W. Diepenbrock, Effects of nitrogen source and rate on productivity and quality of winter oilseed rape (Brassica napus L.) grown in different crop rotations, Field Crops Research, 94 (2005) 103-113.
[46] A.-S. Bouchet, A. Laperche, C. Bissuel-Belaygue, R. Snowdon, N. Nesi, A. Stahl, Nitrogen use efficiency in rapeseed. A review, Agronomy for Sustainable Development, 36 (2016).
[47] S. Li, H. Zhang, S. Wang, L. Shi, F. Xu, C. Wang, H. Cai, G. Ding, The rapeseed genotypes with contrasting NUE response discrepantly to varied provision of ammonium and nitrate by regulating photosynthesis, root morphology, nutritional status, and oxidative stress response, Plant Physiol Biochem, 166 (2021) 348-360.
[48] J.C. Avice, P. Etienne, Leaf senescence and nitrogen remobilization efficiency in oilseed rape (Brassica napus L.), J Exp Bot, 65 (2014) 3813-3824.
[49] H.H. Javed, Y. Hu, M.A. Asghar, M. Brestic, M.A. Abbasi, M.H. Saleem, X. Peng, A.Z. Ghafoor, W. Ye, J. Zhou, X. Guo, Y.C. Wu, Effect of intermittent shade on nitrogen dynamics assessed by (15)N trace isotopes, enzymatic activity and yield of Brassica napus L, Front Plant Sci, 13 (2022) 1037632.
[50] D.J. Harvey, P. Vouros, Mass Spectrometric Fragmentation of Trimethylsilyl and Related Alkylsilyl Derivatives, Mass Spectrom Rev, 39 (2020) 105-211.
[51] W.F. Beshir, V.B.M. Mbong, M. Hertog, A.H. Geeraerd, W. Van den Ende, B.M. Nicolai, Dynamic Labeling Reveals Temporal Changes in Carbon Re-Allocation within the Central Metabolism of Developing Apple Fruit, Front Plant Sci, 8 (2017) 1785.
[52] M. Koubaa, B. Thomasset, A. Roscher, Quantifying 13C-labeling in Free Sugars and Starch by GC-MS, in: M. Dieuaide-Noubhani, A.P. Alonso (Eds.) Plant Metabolic Flux Analysis: Methods and Protocols, Humana Press, Totowa, NJ, 2014, pp. 121-130.

[53] M. Koubaa, S. Mghaieth, B. Thomasset, A. Roscher, Gas chromatography-mass spectrometry analysis of 13C labeling in sugars for metabolic flux analysis, Anal Biochem, 425 (2012) 183-188.
[54] Y. Dellero, O. Filangi, Corrective method dedicated to Isocor for calculating carbon isotopologue distribution from GCMS runs, in, Portail Data INRAE, 2021.
[55] P. Millard, B. Delepine, M. Guionnet, M. Heuillet, F. Bellvert, F. Letisse, IsoCor: isotope correction for high-resolution MS labeling experiments, Bioinformatics, 35 (2019) 4484-4487.
[56] H. Wickham, R. François, L. Henry, K. Müller, dplyr: A Grammar of Data Manipulation, in, 2022.
[57] H. Wickham, M. Girlich, tidyr: Tidy Messy Data, in, 2022.
[58] H. Wickham, ggplot2: Elegant Graphics for Data Analysis, Springer-Verlag New York, 2016.
[59] RStudio Team, RStudio: Integrated Development for R., (2016).
[60] H. Diab, A.M. Limami, Reconfiguration of N Metabolism upon Hypoxia Stress and Recovery: Roles of Alanine Aminotransferase (AlaAT) and Glutamate Dehydrogenase (GDH), Plants (Basel), 5 (2016).
[61] Y. Dellero, C. Mauve, M. Jossier, M. Hodges, The Impact of Photorespiratory Glycolate Oxidase Activity on Arabidopsis thaliana Leaf Soluble Amino Acid Pool Sizes during Acclimation to Low Atmospheric CO2 Concentrations, Metabolites, 11 (2021) 501.
[62] C. Abadie, E.R. Boex-Fontvieille, A.J. Carroll, G. Tcherkez, In vivo stoichiometry of photorespiratory metabolism, Nat Plants, 2 (2016) 15220.
[63] Y. Dellero, M. Jossier, N. Glab, C. Oury, G. Tcherkez, M. Hodges, Decreased glycolate oxidase activity leads to altered carbon allocation and leaf senescence after a transfer from high CO_2 to ambient air in Arabidopsis thaliana, J Exp Bot, 67 (2016) 3149-3163.
[64] Y. Dellero, O. Filangi, A. Bouchereau, Evaluation of GC/MS-Based 13C-Positional Approaches for TMS Derivatives of Organic and Amino Acids and Application to Plant 13C-Labeled Experiments, Metabolites, 13 (2023) 466.
[65] R. Ros, J. Munoz-Bertomeu, S. Krueger, Serine in plants: biosynthesis, metabolism, and functions, Trends Plant Sci, 19 (2014) 564-569.
[66] T.D. Sharkey, Pentose Phosphate Pathway Reactions in Photosynthesizing Cells, Cells, 10 (2021).
[67] A.L. Preiser, N. Fisher, A. Banerjee, T.D. Sharkey, Plastidic glucose-6-phosphate dehydrogenases are regulated to maintain activity in the light, Biochem J, 476 (2019) 1539-1551.
[68] J. Joshi, J.S. Amthor, D.R. McCarty, C.D. Messina, M.A. Wilson, A.H. Millar, A.D. Hanson, Why cutting respiratory CO_2 loss from crops is possible, practicable, and prudential, Modern Agriculture, (2023) 11.
[69] M. Rahim, M. Ragavan, S. Deja, M.E. Merritt, S.C. Burgess, J.D. Young, INCA 2.0: A tool for integrated, dynamic modeling of NMR- and MS-based isotopomer measurements and rigorous metabolic flux analysis, Metab Eng, 69 (2022) 275-285.
[70] S. Koley, K.L. Chu, S.S. Gill, D.K. Allen, An efficient LC-MS method for isomer separation and detection of sugars, phosphorylated sugars, and organic acids, J Exp Bot, 73 (2022) 2938-2952.
[71] B.M. O'Leary, C.P. Lee, O.K. Atkin, R. Cheng, T.B. Brown, A.H. Millar, Variation in Leaf Respiration Rates at Night Correlates with Carbohydrate and Amino Acid Supply, Plant Physiol, 174 (2017) 2261-2273.
[72] B.M. O'Leary, G.G.K. Oh, C.P. Lee, A.H. Millar, Metabolite Regulatory Interactions Control Plant Respiratory Metabolism via Target of Rapamycin (TOR) Kinase Activation, Plant Cell, 32 (2020) 666-682.
[73] L. Furtauer, W. Weckwerth, T. Nagele, A Benchtop Fractionation Procedure for Subcellular Analysis of the Plant Metabolome, Front Plant Sci, 7 (2016) 1912.
[74] L. Furtauer, L. Kustner, W. Weckwerth, A.G. Heyer, T. Nagele, Resolving subcellular plant metabolism, Plant J, 100 (2019) 438-455.
[75] A. Destailleur, T. Poucet, C. Cabasson, A.P. Alonso, J.C. Cocuron, R. Larbat, G. Vercambre, S. Colombie, P. Petriacq, M.H. Andrieu, B. Beauvoit, Y. Gibon, M. Dieuaide-Noubhani, The Evolution of Leaf Function during Development Is Reflected in Profound Changes in the Metabolic Composition of the Vacuole, Metabolites, 11 (2021).

[76] D.K. Allen, Quantifying plant phenotypes with isotopic labeling & metabolic flux analysis, Curr Opin Biotechnol, 37 (2016) 45-52.
[77] X.H. Le, A.H. Millar, The Diversity of Substrates for Plant Respiration and How to Optimize Their Use, Plant Physiol, (2022).
[78] S. Timm, A. Nunes-Nesi, A. Florian, M. Eisenhut, K. Morgenthal, M. Wirtz, R. Hell, W. Weckwerth, M. Hagemann, A.R. Fernie, H. Bauwe, Metabolite Profiling in Arabidopsisthaliana with Moderately Impaired Photorespiration Reveals Novel Metabolic Links and Compensatory Mechanisms of Photorespiration, Metabolites, 11 (2021).
[79] V.M. Andriotis, M.J. Pike, S. Bunnewell, M.J. Hills, A.M. Smith, The plastidial glucose-6-phosphate/phosphate antiporter GPT1 is essential for morphogenesis in Arabidopsis embryos, Plant J, 64 (2010) 128-139.
[80] F. Facchinelli, A.P. Weber, The metabolite transporters of the plastid envelope: an update, Front Plant Sci, 2 (2011) 50.
[81] L.J. Sweetlove, T.C. Williams, C.Y. Cheung, R.G. Ratcliffe, Modelling metabolic CO(2) evolution--a fresh perspective on respiration, Plant Cell Environ, 36 (2013) 1631-1640.
[82] V.G. Maurino, Using energy-efficient synthetic biochemical pathways to bypass photorespiration, Biochem Soc Trans, 47 (2019) 1805-1813.
[83] P.F. South, A.P. Cavanagh, H.W. Liu, D.R. Ort, Synthetic glycolate metabolism pathways stimulate crop growth and productivity in the field, Science, 363 (2019) 11.
[84] J.E. Lunn, Compartmentation in plant metabolism, J Exp Bot, 58 (2007) 35-47.
[85] A.R. Fernie, F. Carrari, L.J. Sweetlove, Respiratory metabolism: glycolysis, the TCA cycle and mitochondrial electron transport, Curr Opin Plant Biol, 7 (2004) 254-261.
[86] S. Wulfert, S. Krueger, Phosphoserine Aminotransferase1 Is Part of the Phosphorylated Pathways for Serine Biosynthesis and Essential for Light and Sugar-Dependent Growth Promotion, Front Plant Sci, 9 (2018) 1712.
[87] B. Cascales-Minana, J. Munoz-Bertomeu, M. Flores-Tornero, A.D. Anoman, J. Pertusa, M. Alaiz, S. Osorio, A.R. Fernie, J. Segura, R. Ros, The phosphorylated pathway of serine biosynthesis is essential both for male gametophyte and embryo development and for root growth in Arabidopsis, Plant Cell, 25 (2013) 2084-2101.
[88] R.M. Benstein, K. Ludewig, S. Wulfert, S. Wittek, T. Gigolashvili, H. Frerigmann, M. Gierth, U.I. Flugge, S. Krueger, Arabidopsis phosphoglycerate dehydrogenase1 of the phosphoserine pathway is essential for development and required for ammonium assimilation and tryptophan biosynthesis, Plant Cell, 25 (2013) 5011-5029.
[89] W. Toujani, J. Munoz-Bertomeu, M. Flores-Tornero, S. Rosa-Tellez, A.D. Anoman, S. Alseekh, A.R. Fernie, R. Ros, Functional characterization of the plastidial 3-phosphoglycerate dehydrogenase family in Arabidopsis, Plant Physiol, 163 (2013) 1164-1178.
[90] A.U. Igamberdiev, L.A. Kleczkowski, The Glycerate and Phosphorylated Pathways of Serine Synthesis in Plants: The Branches of Plant Glycolysis Linking Carbon and Nitrogen Metabolism, Front Plant Sci, 9 (2018) 318.
[91] Y. Zhang, A. Sampathkumar, S.M. Kerber, C. Swart, C. Hille, K. Seerangan, A. Graf, L. Sweetlove, A.R. Fernie, A moonlighting role for enzymes of glycolysis in the co-localization of mitochondria and chloroplasts, Nat Commun, 11 (2020) 4509.
[92] R. Boldt, C. Edner, U. Kolukisaoglu, M. Hagemann, W. Weckwerth, S. Wienkoop, K. Morgenthal, H. Bauwe, D-GLYCERATE 3-KINASE, the last unknown enzyme in the photorespiratory cycle in Arabidopsis, belongs to a novel kinase family, Plant Cell, 17 (2005) 2413-2420.